Journal of Dynamic Behavior of Materials
https://doi.org/10.1007/s40870-025-00468-8

RESEARCH PAPER

Dynamic Spall Failure of Polymers

K. G. Frawley[1] · G. Kennedy[1] · J. L. Jordan[2] · R. Ramprasad[1] · N. N. Thadhani[1]

Received: 25 July 2024 / Accepted: 22 February 2025
© The Author(s) 2025

Abstract

The dynamic tensile spall failure strength of polymers subjected to high-pressure shock compression and high-strain-rate deformation is of increasing interest across a wide range of applications in extreme environments. Currently, there is no expansive database of polymeric materials for which spall strength properties are available. Plate-on-plate impact gas gun experiments were performed on 11 commercially available polymers using a multi-sample target configuration. The spall strengths obtained from velocity profiles captured using Photon Doppler Velocimetry interferometry for these polymers range from 25 to 160 MPa, with no direct correlation to their inherent characteristics, including the amorphous/semi-crystalline structure. A database of the spall strengths of 23 unique polymers, experimentally determined in this work and combined with those available in the literature, was created to include readily available mechanical and physical properties of the various polymers. The spall strength of most polymers is found to be typically higher than the corresponding quasi-static compressive and tensile strength values and about 30–50% of their bulk and elastic moduli, with some exceptions. Normalizing the spall strengths of the various polymers with respect to their calculated theoretical strength, and then correlating with their decompression (tensile) strain rate, reveals consistent trends similar to those for metals and alloys. Namely, the normalized spall strengths are nominally within 20% of the theoretical strength, although no obvious distinction between the spall failure response of the various polymer types based on amorphous or semi-crystalline structure is observed.

Keywords Spall strength · Polymers · Plate-on-plate impact experiments

Introduction

The dynamic mechanical behavior of materials subjected to high-velocity impacts, explosions, and seismic events is important across a wide range of applications in commercial, military, mining, and geological sectors. It is also of scientific importance for understanding the structure–property correlations in materials subjected to high-pressure shock compression and high strain rate deformation, particularly relevant to guiding their design for such extreme environments. The dynamic tensile, or "spall" failure, is a kinetically evolving internal rupture process occurring via void/crack nucleation, growth, and coalescence. It occurs when impact-generated shock waves propagating and reflecting at free surfaces produce rarefaction (release) waves that interact, producing internal tensile stresses exceeding the tensile strength of the material. The measure of a material's resistance to such tension-induced internal failure (or rupture) is defined as the spall strength [1], a critical property often considered to determine the performance of materials during extreme conditions of high-velocity impact associated with automotive crashes, structural barriers, space debris impact, and ballistics [2–6].

Shock compression preceding the buildup of internal tension can cause plastic deformation at strain rates exceeding 10^5 s^{-1} and can significantly alter the pre-existing microstructure, creating sites for spall-induced void/crack nucleation. While prior research and understanding of spall strength and failure processes have primarily concentrated on metals and alloys (through experiments and/or computational simulations) [7–10], there have been only limited studies performed on polymers [11–14]. Polymers present increasing opportunities for use in crafting lightweight,

---

J. L. Jordan is a member of SEM.

N. N. Thadhani
naresh.thadhani@mse.gatech.edu

[1] School of Materials Science and Engineering, Georgia Institute of Technology, 771 Ferst Drive NW, Atlanta, GA 30332, USA

[2] Los Alamos National Laboratory, Los Alamos, NM 87545, USA

Published online: 12 March 2025

impact-resistant armors and protective shells for containing explosive devices, among other applications [15]. Furthermore, the deformation and failure characteristics of fully amorphous or semi-crystalline polymers under shock compression and high strain rates can be markedly different due to their uniform micro- and meso-scale structures, compared to those of metals and alloys [16].

The primary method for spall strength determination is through measurements of free surface velocity profiles, commonly obtained using time-resolved optical interferometry during gun-launched plate-on-plate impact, explosive charges, and pulsed laser experiments. The free surface velocity profiles capture characteristic signatures: rapid loading to peak shock state, unloading, reloading with velocity pullback (resulting from spall failure), followed by continued wave reverberations. The magnitude of the pullback from the steady-state peak velocity provides the measure of the spall strength. Various shock-loading techniques generate different peak states, durations, and strain rates, which can lead to different spall failure responses and properties. In particular, spall strengths are higher at higher strain rates (10^6–10^9 s^{-1}) typically obtained with explosive and laser shock experiments, in comparison to strain rates obtained in gun-launched plate-on-plate impact experiments (10^4–10^6 s^{-1}). Variations in spall strengths are also often seen with increasing impact stress, in part due to microstructural alterations caused by shock compression preceding the generation of tension, although the trend is more obvious in metals and alloys. The higher degree of compression of polymers (in comparison to metals) can influence the rate of deformation and in turn affect the rate dependence of spall strength [16].

The response of polymers to shock compression and high strain rate loading is dependent on several factors, including polymer type (thermoset or thermoplastic, glassy or rubbery, and amorphous or semi-crystalline), as well as processing and impact conditions. Thermoset polymers undergo irreversible crosslinking upon cooling, rendering them unable to be reshaped through reheating. In contrast, thermoplastics retain their ability to be reshaped upon heating. A comparative study utilizing PTFE and KEL-F-800 as thermoplastics and Estane as a thermosetting polymer reveals distinctly different dynamic behaviors between the two classes [17]. Similarly, the shock compression responses of polyethylene (PE), polytetrafluorethylene (PTFE), polycarbonate (PC), and epoxy (XB3485 resin and 3486 hardener) have been shown to exhibit distinct differences in behaviors under weak (low-pressure) shock loading, due to their capacity to overcome interchain interactions (Van der Waals forces) [15]. The different behaviors delineate the response of thermosetting polymers, characterized by extensive crosslinking, from thermoplastics that lack such structures. At higher shock pressures, however, the influence of crosslinking diminishes, leading to a convergence in the behavior between thermoplastics and thermosetting polymers, with both exhibiting similar responses.

Additionally, two-part epoxies such as those created by polymerizing the EPON 828 resin exhibit differing spall responses depending on the curing agent used, which influences the cross-linking process within the polymer matrix [18]. Some polymers also demonstrate spall strengths that are unaffected by processing and impact loading conditions. Notably, as demonstrated by Jordan et al. [19, 20], high-density polyethylene (HDPE) exhibits consistent dynamic failure response with spall strength values of 50–70 MPa at impact velocities of 428–800 m/s. On the other hand, more recent work on ultra-high molecular weight polyethylene (UHMWPE) has shown nearly constant spall strength of ~ 70 MPa at impact pressures up to 0.9 GPa, followed by a continuous decrease in spall strength to ~ 30 MPa at higher shock stresses of about 2.0 GPa [21].

A limited number of computational studies using molecular dynamics (MD) simulations have been performed on polymers to provide a molecular-level understanding of the spall failure mechanism and to determine the spall strength. Dewapriya and Miller [22, 23], using large-scale MD simulations, showed that the spall strength of amorphous polymers (polyurethane and polyurea) computed from simulated free surface velocity histories correlates with fracture nucleation stress rather than the quasi-static tensile strength. In another more recent study on amorphous PE [24], which does not contain cyclic structures in its monomer (unlike polyurethane and polyurea), the same authors simulated the impact of a slab of PE molecules at a higher velocity and calculated the corresponding free surface velocity history. The spall strength computed from their simulated velocity profiles showed values consistently and significantly lower than the actual buildup of tensile stresses in the spalled region.

In this paper, we present results of spall strength measurements on several commonly used polymers, including two (HDPE and PET) that have been previously studied [19, 25]. The measurements involve gas gun plate-on-plate impact experiments using a multi-sample target configuration and Photon Doppler Velocimetry (PDV) to obtain the free surface velocity profiles and determine the pullback velocity as the measure of the spall strength. The spall strengths of polymers determined in this work are combined with those of polymers documented in the literature to establish a database of over 20 polymers. The spall properties of these polymers are compared with routinely available properties to determine trends correlating quasi-static and dynamic behavior of polymeric materials. Comparisons among different polymeric systems are also mapped, considering the spall strength normalized with their theoretical strength as a function of the decompression (tensile) strain rate, which

Table 1 Polymers investigated listing the type, brand, and measured values of their respective density and sound speed values

Material—Brand—Form	Density, $\rho(g/cm^3)$	Longitudinal wave speed, $c_l(m/s)$	Shear wave speed, $c_s(m/s)$	Bulk wave speed, $c_b(m/s)$
Acrylonitrile butadiene styrene (ABS) Absylux®—*Amorphous thermoplastic*	1.031	2210	911	1944
Chlorinated polyvinyl chloride (CPVC) Corzan®—*Amorphous thermoplastic*	1.441	2143	1014	1795
High density polyethylene (HDPE) Densetec®[a]—*Semi-crystalline thermoplastic*	0.941	2440	1016	2139
Polyetherimide (PEI) ULTEM 1000—*Amorphous thermoplastic*	1.243	2485	1060	2163
Polyester, or polyethylene terephthalate (PET) Celanex®—*Semi-crystalline thermoplastic*	1.354	2441	1023	2136
Polyoxymethylene (POM) Delrin®—*Semi-crystalline thermoplastic*	1.405	2383	983	2095
Polypropylene (PP) Propylux®—*Semi-crystalline thermoplastic*	0.916	2583	1273	2124
Polyphenylene Oxide (PPO) Noryl®—*Amorphous thermoplastic*	1.049	2258	999	1941
Polyphenylene sulfide (PPS) Techtron®—*Semi-crystalline thermoplastic*	1.326	2483	1046	2169
Polyphenylsulfone (PPSU) Radel® R5500—*Amorphous thermoplastic*	1.271	2264	860	2034
Polyvinylidene fluoride (PVDF) Solef®—*Semi-crystalline fluoropolymer*	1.730	2024	972[b]	1684[b]

[a] Provided by Los Alamos National Laboratory

[b] Sample unable to support shear waves; hence, sound speeds calculated using Poisson's ratio of 0.327 [26]

represents the rate of material expansion during unloading from the high-pressure state.

Materials and Methods

Table 1 lists the various thermoplastic amorphous and semi-crystalline polymers experimentally investigated in this work. The polymers were commercially acquired in the form of plates, from which disk-shaped samples were machined for the impact experiments. The density of each polymer sample disk was measured using the Archimedes method, and their ultrasonic sound speeds were measured using transducers oriented normal to the in-plane direction of the plate. The longitudinal wave speed ($\boldsymbol{C_L}$) was measured using a VSP 200 pressure transducer, while shear wave speed ($\boldsymbol{C_S}$) was measured using an SRD50-5 Ultron pressure transducer with an Olympus 5072PR pulsar/receiver in the pulse echo configuration and a Tektronix DPO 5104 1 GHz Oscilloscope. The bulk wave speed was calculated from the measured longitudinal and shear wave velocities. Values of the density and elastic wave velocities for each polymer are listed in Table 1.

The spall strengths of the various polymers were determined using plate-on-plate impact experiments performed with the 80 mm diameter barrel single-stage gas gun at Georgia Tech. Figure 1a shows a schematic of the impact experiment geometry illustrating a polyurethane foam-supported ($\rho = 0.32$ g/cm^3) HDPE flyer plate (2.5 mm thickness and 70 mm diameter) mounted on an aluminum sabot, impacting the sample holding target assembly. Two types of multi-sample target configurations (three-sample and seven-sample) illustrated schematically in Fig. 1b and c were used. The three-sample configuration (Fig. 1b) was used with HDPE sample disks machined from the different x-, y-, and z-orientations of a 5 cm thick slab,[1] to determine if orientation effects associated with the manufacturing of the slab influence the spall strength. A collimated PDV probe with 1 mm housing size (AC Photonics P/N: 1CL15P020LCB01) was placed on the back of each of the three samples. An additional focusing probe with 8 mm housing size (Oz Optics P/N: LPF-04-1550-9/125-S-1.6-48-18AS-60-3A-1–2) probe was also placed on the back of the through-thickness (or x-orientation) sample to determine the effect of the probe size. The experiment was performed at an impact velocity of ~ 430 m/s, with each of the three target sample disks of thickness of 5 mm and diameter of 25 mm embedded in a PMMA surround ring.

For the seven-sample configuration (Fig. 1c), the disk-shaped samples were cut from commercially acquired sheets of approximately 7 mm thickness to a diameter of 25 mm.

---

[1] Same HDPE slab as that used in the work by Jordan et al. [19].

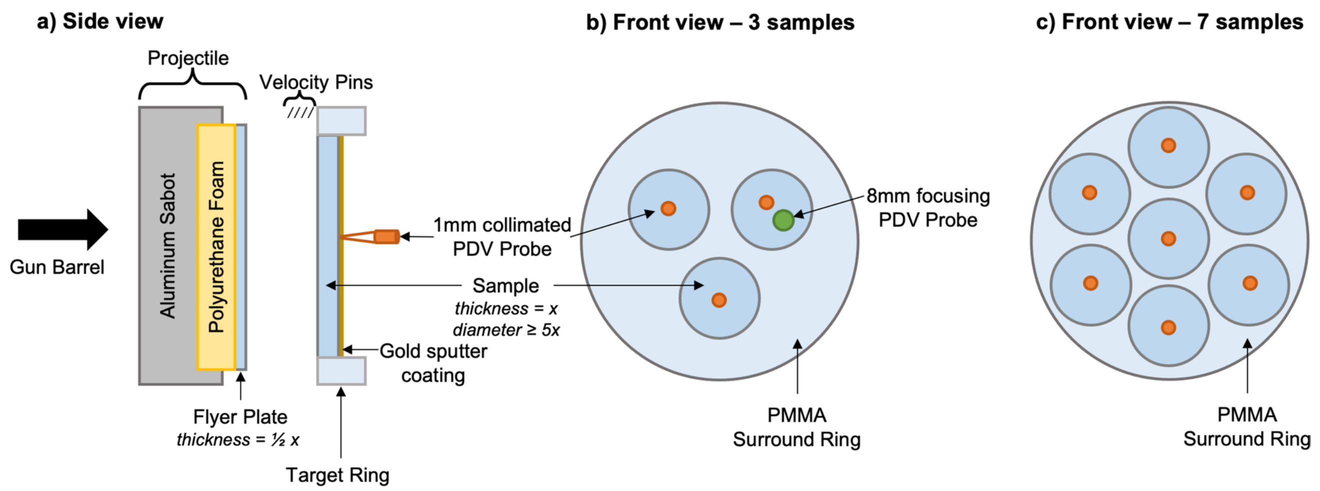

Fig. 1 Sketch of the experimental setup for the multi-sample configuration showing **a** the side view of the projectile impacting the target ring of **b** 3-sample and **c** 7-sample configurations

Similar to the three-sample target configuration, a foam-supported HDPE flyer of 3.3 mm thickness impacted the samples at velocities of ~ 430 m/s. A 1 mm collimated PDV probe was placed on the back of each sample. For some experiments, the back free surface of each sample was sputter coated with a gold layer to improve reflectivity.

The PDV probes in both experimental configurations were connected to a mixed multiplex PDV (MPDV) system capable of conventional, time-delayed, and frequency up-shifted measurements. A 1 km long SMF-28 fiber optic cable created a ~ 5 µs time delay in simultaneous impact events, while frequency separations of ~ 2 GHz and ~ 4 GHz were used to upshift the frequency of captured signals. A PDV probe positioned orthogonally to, and flush with, the impact surface was also used to determine the impact velocity $\left(\boldsymbol{V_{impact}}\right)$ with an accuracy of 0.1%. A series of four electrically charged pins of known spacing were attached approximately 50 mm in front of the target plate to trigger the digitizer and collect the PDV data, as well as a backup measurement of the impact velocity. The PDV signals were collected using a Teledyne Lecroy WaveMaster 813Zi-B 13 GHz Oscilloscope. The data analysis was performed using HiFiPDV [27], applying a range of window functions, duration/time bins, and peak determination methods to find the best fit and uncertainty for the velocity at each point in the profile. A typical free surface velocity profile obtained from a plate-on-plate impact experiment as the shock wave propagates through the polymer target displays an initial increase to a steady-state peak velocity, followed by a decrease (decompression) until tension-induced spall failure causes a pullback in velocity, followed by recompression and ringing in the spalled region. The stresses corresponding to the peak velocity state ($\boldsymbol{\sigma_{peak}}$) and the spall strength ($\boldsymbol{\sigma_{SPALL}}$) obtained from the pullback are calculated using Eqs. (1) [16] and (2) [28], where $\boldsymbol{\rho_0}$ is the initial density, $\boldsymbol{C_L}$ is longitudinal sound speed, $\boldsymbol{V_{peak}}$ is peak velocity, $\boldsymbol{C_0}$ is the bulk sound speed, and $\boldsymbol{\Delta u_{fs}}$ is the change in the free surface velocity from the peak velocity to the pullback trough observed in the measured profiles.

$$\sigma_{peak} = \frac{1}{2}\rho_0 C_l \mathrm{V}_{\mathrm{peak}} \tag{1}$$

$$\sigma_{SPALL} = \frac{1}{2}\rho_0 C_0 \Delta u_{fs} \tag{2}$$

The decompression (tensile) strain rate ($\acute{\epsilon}$), also known as the volume rate of material expansion, is given by Eq. (3), where $\boldsymbol{\Delta \dot{u}_{fs}}$ is the rate of change of the pullback velocity and $\boldsymbol{C_0}$ is the bulk sound speed [28]:

$$\acute{\epsilon} = \frac{1}{2}\frac{\Delta \dot{u}_{fs}}{C_0} \tag{3}$$

Results and Discussion

Spall Properties of Polymers from Experiments Under Similar Impact Conditions

Three sets of gas gun plate-on-plate impact experiments were performed using the three- and seven-sample target configurations at impact velocities of about 430 m/s. The measured PDV velocity profiles obtained from the first experiment performed on HDPE (disks of different plate orientations) using the three-sample target configuration at an impact velocity of 433 m/s are shown in Fig. 2a and b. The velocity profiles in Fig. 2a illustrate no effect of impact

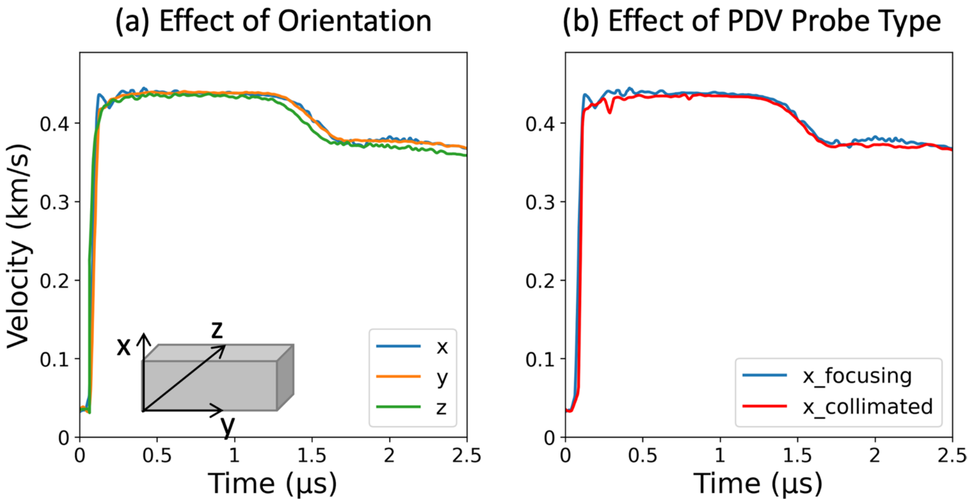

Fig. 2 Velocity profiles for HDPE obtained from **a** samples of three different orientations of a plate and **b** two different types of PDV probes

orientation relative to the samples sectioned from different orientations of the HDPE slab. The near-identical signatures are independent of sample orientation, showing similar rapid rise time and duration of peak state, decompression, and pullback characteristics with no significant velocity increase upon recompression. Hence, it is seen that HDPE exhibits no evidence of asymmetric orientation-dependent behavior. Figure 2b shows velocity profiles captured by both the 1 mm collimated and 8 mm focusing PDV probes, also revealing identical responses. The spall strengths of the three HDPE samples calculated from the velocity profiles obtained from this experiment are 65–70 MPa, which are in the same range of values reported by Jordan et al. [19] on HDPE at different impact velocities. The similarity of measured velocity profiles and spall strength values is indicative of a lack of dependence of the spall response on impact conditions, as well as on directional anisotropy that may otherwise be influenced by the polymer fabrication process.

Two additional experiments were performed using the seven-sample target assembly at 429 m/s on PET, POM, and PP polymers, and at 427 m/s on ABS, CPVC, PEI, PPO, PPS, PPSU, and PVDF polymers. The measured velocity profiles obtained from the corresponding PDV probes for all polymer samples investigated (including HDPE) are shown in Fig. 3. It can be seen that in all cases, the velocity profiles reveal the similar initial rise to a steady-state peak and plateau, followed by a gradual decrease (decompression) and velocity pullback indicative of spall failure. The profiles for CPVC, PEI, PET, and PP show recompression following velocity pullback, while none or weak recompression is observed for ABS, HDPE, POM, PPO, PPS, PPSU, and PVDF. The gradual release (decrease in velocity) from the peak state is indicative of slow, or “viscous,” ductile tensile fracture [11, 12, 16, 17]. The various atypical responses observed in our work, such as the pullback signal illustrating decompression followed by lack of recompression and ringing, are not different from those seen in the literature. While recompression is indicative of void nucleation, growth, and coalescence processes, it is likely that the low strength of the polymer is not able to support further recompression and ringing, and therefore the velocity profile in some cases shows a flat or even decreasing slope. For the purpose of this work, we determined the spall strength considering the pullback velocity based on the peak and the point at which a change in slope is seen following the decompression. Only in the case of PPSU, the velocity profile shows an abrupt end point following decompression, which we considered for determining as the pullback velocity. The rise time to peak velocity as seen in the PDV profiles for each of the impacted polymers is relatively similar (0.1–0.3 μs), which is an order of magnitude longer than that for metals (~0.01 μs) at similar impact conditions. This could be because of shock wave dispersion as it propagates through the relatively convoluted molecular structure of polymers, including chains and cross-linked molecules, as well as the inherent free volume of the amorphous structure.

Table 2 lists the various measured parameters (impact velocity, rise time, and peak and pullback velocities) as well as the calculated values of the peak stress, spall strength, and decompression strain rate obtained using Eqs. (1–3). The error ranges indicated for each set of calculated data represent uncertainty in the measured values. This uncertainty is determined by the fluctuations in peak velocity shown in the profiles in Fig. 3, which in turn affects the spall strength, peak stress, and decompression strain rate.

It can be seen that under similar impact velocity conditions (~430 m/s), the rise time to peak state ranges from 0.11 to 0.27 μs with no obvious correlation with the semicrystalline or amorphous characteristics of the various polymers investigated. The peak stress range of 468 to 566 MPa, corresponding to peak free surface velocities of 318 to 438 m/s, is affected by the shock impedance (product of density

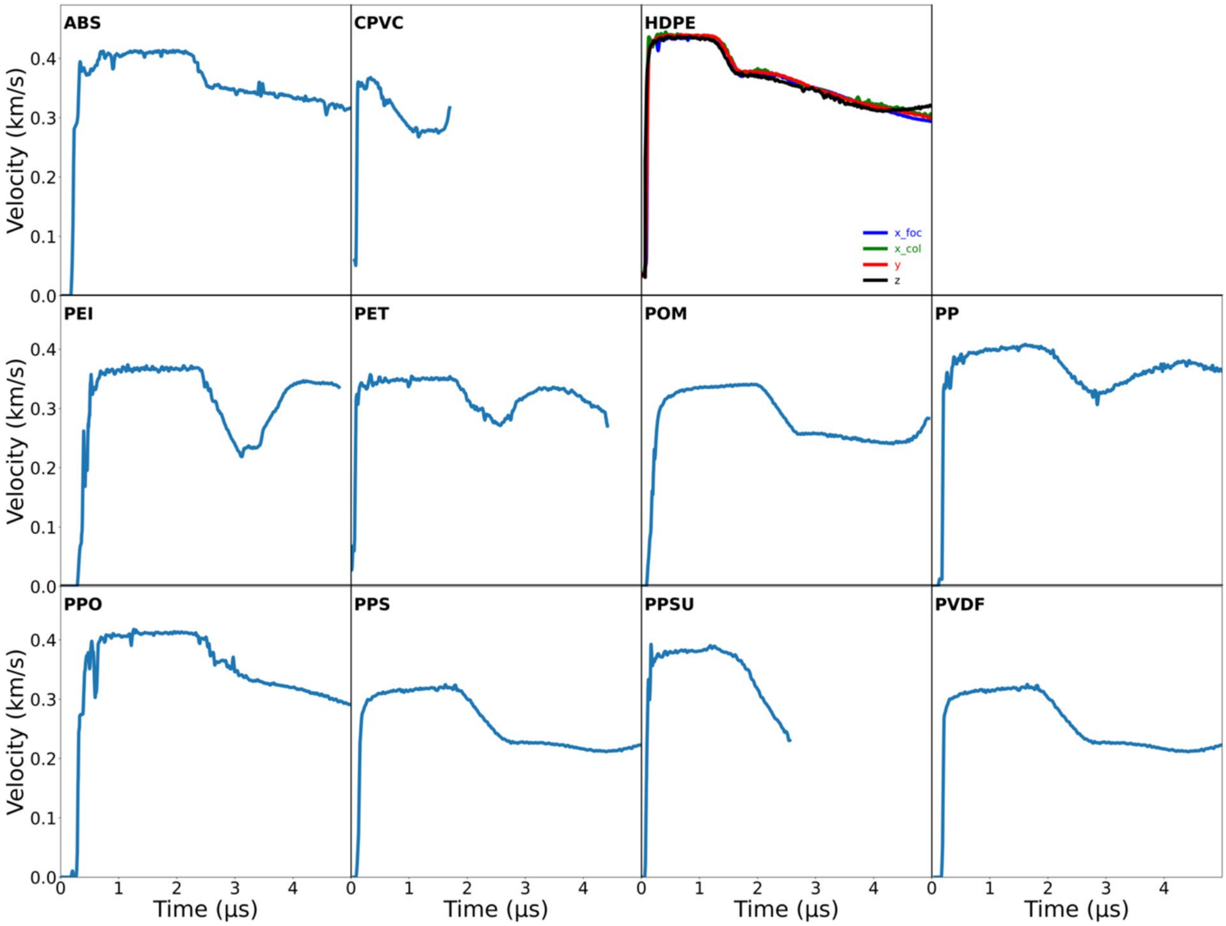

Fig. 3 PDV velocity profiles measured from the plate-impact gas gun experiments performed on the 11 polymers investigated in this work. HDPE has multiple traces because of the experiment performed on samples from the three different orientations of the plate. Some of the velocity profiles (e.g., for CPVC and PPSU) end abruptly due to time-delay since the data collection of the next multiplexed probe starts and cuts off the data from the prior probe prior to recompression. The velocity profiles for CPVC, PEI, PET, and PP show recompression following velocity pullback, while only weak recompression (or none) is observed for ABS, HDPE, POM, PPO, PPS, PPSU, and PVDF

and shock speed). The rate of release from the peak velocity, or decompression (tensile) strain rate, is indicative of the rate of material expansion upon release. Polymers experiencing similar impact velocity conditions show a range of decompression strain rates from 2×10^4 to 5.3×10^4 s^{-1}. Figure 4 plots the calculated values of the peak stress (top) and spall strength (bottom) versus the calculated decompression strain rate for the various polymers based on the experiments performed in this work. It can be seen that while multiple HDPE samples (blue circles) impacted in the same experiment (Shot 2101) show almost similar values of peak stress and spall strength with small variation in decompression strain rate, the three polymers PET, POM, and PP (orange circles) also impacted in the same experiment (Shot 2301) show variations in peak stress and decompression strain rate but similar spall strength. The seven polymers (green circles and triangles) impacted in the same experiment (Shot 2305) show widely varying values of peak stress, spall strength, and decompression strain rate, independent of their amorphous (triangles) and semi-crystalline (circles) structure states. Hence, no obvious effects of structural (semi-crystalline or amorphous) characteristics or correlations are revealed from the variation of the peak stress and spall strength as a function of the decompression strain rate for the polymers investigated.

The spall strength, or the ability to withstand internal tensile rupture, obtained from the measured pullback velocity for amorphous polymers is found to be in the range of 64 MPa on the low end for ABS and PPO to 160 MPa on the high end for PEI, while for semi-crystalline polymers it ranges from 25 MPa on the low end for PPS to 100 MPa for PVDF. Most polymers have spall strength values in the 60–90 MPa range. It should be noted that the decompression strain rate and spall strength are specific for each polymer

Table 2 Measured parameters including rise time, and peak and pullback velocities, and calculated values of peak stress, spall strength, and decompression strain rate obtained from the three plate impact experiments performed on all polymer samples (A-Amorphous, S-Semicrystalline) investigated

Experiment number	Target material	Rise time (μs)	Peak velocity (m/s)	Peak stress (MPa)	Decompression strain rate × 10^4 ($1/s$)	Δu_{fs} (m/s)	σ_{sp} (MPa)
2101 @ 433 m/s	S-HDPE$_{x\text{-}f}$	0.22 ± 0.07	434 ± 1	548 ± 1	3.0 ± 0.0	64 ± 1	69 ± 1
	S-HDPE$_{x\text{-}c}$	0.26 ± 0.01	438 ± 4	553 ± 2	3.0 ± 0.1	62 ± 2	68 ± 2
	S-HDPE$_y$	0.22 ± 0.04	438 ± 3	553 ± 3	2.9 ± 0.1	61 ± 2	66 ± 2
	S-HDPE$_z$	0.22 ± 0.09	435 ± 6	549 ± 4	3.4 ± 0.2	60 ± 3	66 ± 4
2301 @ 423 m/s	S-PET	0.16 ± 0.09	349 ± 4	573 ± 5	2.3 ± 0.1	77 ± 3	84 ± 3
	S-POM	0.25 ± 0.08	340 ± 4	554 ± 4	2.9 ± 0.1	83 ± 2	90 ± 3
	S-PP	0.27 ± 0.01	404 ± 8	480 ± 5	2.1 ± 0.1	81 ± 4	88 ± 5
2305[a] @ 427 m/s	A-ABS	0.16 ± 0.09	410 ± 4	468 ± 3	5.3 ± 0.3	59 ± 3	64 ± 3
	A-CPVC	0.13 ± 0.05	364 ± 19	563 ± 25	3.8 ± 0.7	87 ± 16	94 ± 17
	A-PEI	0.24 ± 0.09	366 ± 10	566 ± 8	4.7 ± 0.2	147 ± 5	160 ± 6
	A-PPO	0.27 ± 0.08	412 ± 6	488 ± 5	2.5 ± 0.2	59 ± 4	64 ± 4
	S-PPS	0.20 ± 0.02	318 ± 9	524 ± 10	3.1 ± 0.9	23 ± 6	25 ± 7
	A-PPSU	0.11 ± 0.09	382 ± 11	549 ± 12	4.2 ± 0.4	79 ± 8	86 ± 9
	S-PVDF	0.14 ± 0.03	319 ± 12	558 ± 13	3.1 ± 0.2	92 ± 7	100 ± 8

The error bars for rise time and peak velocity were calculated based on fluctuations (min/max) in velocity; those for peak stress, decompression strain rate, velocity pullback, and spall strength were determined based on the variations in peak velocity (min/max)

[a] For all samples in this experiment, the back free surface of each sample was sputter coated with a gold layer to improve reflectivity

and not a consequence of varying impact conditions, since the data obtained for each polymer is based on experiments performed at the same nominal impact velocity.

The velocity pullback characteristic of the wave profiles and calculated values of spall strength appear to be indicative of ductile failure response for the amorphous and semi-crystalline polymers investigated in this work. Grady [1] formulated an equation to calculate the theoretical spall strength of ductile materials, considering an energy balance model accounting for the work done and energy dissipated in the activation, growth, and coalescence of voids. The model assumes that the spall strength for ductile materials is independent of strain rate, since the latter only provides a consideration of the time factor during which spall occurs. The theoretical spall strength according to Grady's model is given by Eq. (4), where $\boldsymbol{\rho c_0^2}$ is the compressibility (or bulk modulus), $\boldsymbol{Y}$ is the flow stress (or yield strength), and $\boldsymbol{\varepsilon_c}$ is the critical void volume fraction. For ductile polycrystalline metals and alloys, $\boldsymbol{\varepsilon_c} = 0.15$.

$$P_s = \left(2\rho c_0^2 Y \varepsilon_c\right)^{1/2} \tag{4}$$

Grady's model does not include dependence on microstructure-dominated material properties, though some more recent models for metals account for microstructure. Nevertheless, for homogeneous single-phase materials, it provides a reasonable estimate of spall strength compared to measured values for various metals and alloys [1]. Considering that the spall response of polymer systems is different from that of metals, we nevertheless applied Eq. (4) to calculate the critical void volume fraction ($\boldsymbol{\varepsilon_c}$) at spall for the polymers investigated in this work. We assumed ductile spall behavior and used the actual measured spall strength values along with the values of the bulk modulus and quasi-static yield strength (see the Appendix for Table 3 of properties) of various polymers. The calculations reveal that the critical void volume fraction ($\boldsymbol{\varepsilon_c}$) at spall is not constant for polymers, unlike that for metals and alloys. For amorphous polymers, $\boldsymbol{\varepsilon_c}$ is in the range of 0.01 for PPS to 0.24 for PVDF, while that for semi-crystalline polymers is in the range of 0.12 for ABS to 0.35 for POM. The variability and wide range of the critical void volume fraction at spall for polymers could be associated with the viscous fracture and lack of effects of stress concentration initiating spall-induced void nucleation typically seen with metals and alloys.

Combined Spall Data from Current Experiments and Literature

In addition to the polymers investigated in this study, we catalogued other polymers from the literature [17–19, 24, 28] for which the data on spall strength measurements performed only using gas gun plate-on-plate impact experiments, essentially within the same strain rate range, are available. Figure 5 shows a plot that includes the compilation of the spall strengths of a total of 23 different

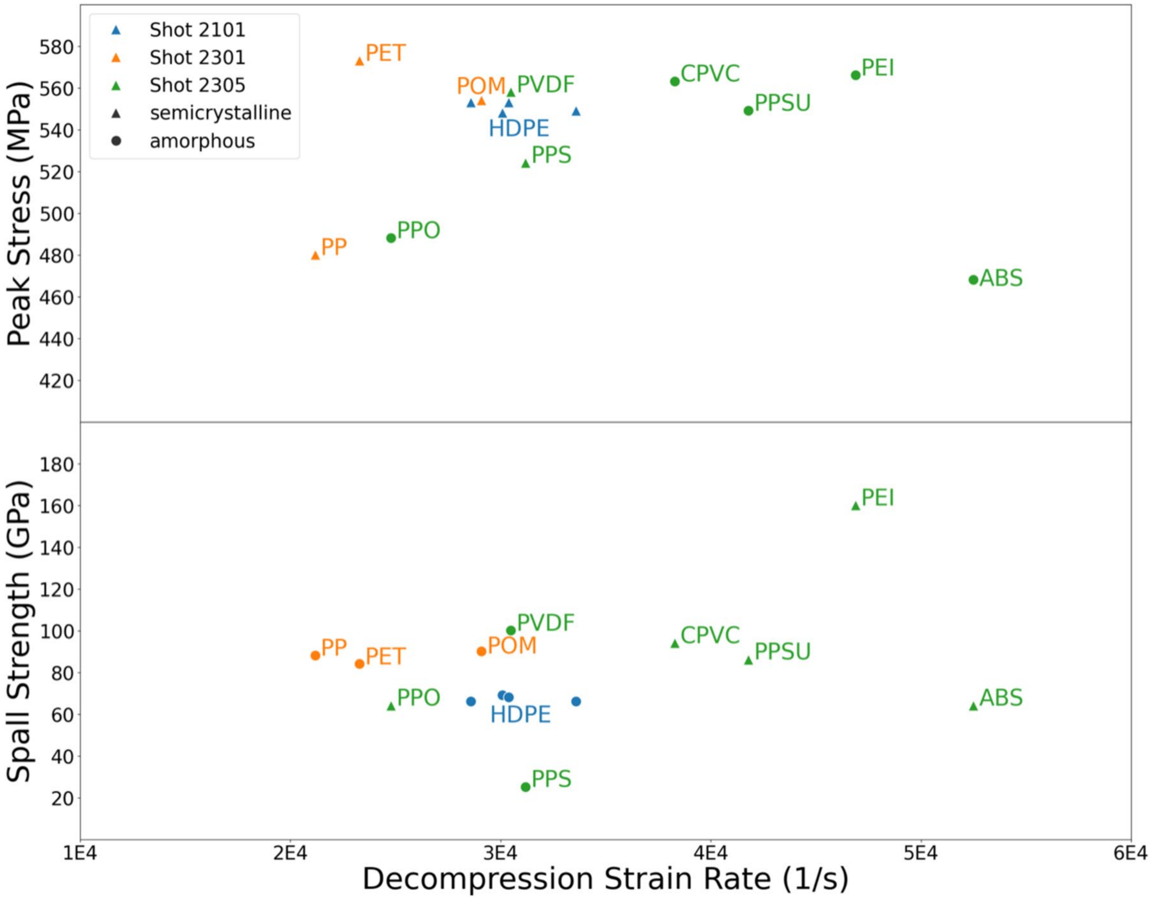

Fig. 4 Experimentally determined values of peak stress (top) and spall strength (bottom) correlated with decompression strain rate for various polymers. The data points are color coded with respect to the samples being simultaneously impacted using multi-sample target assembly (all three experiments performed at same approximate impact velocity) and different symbols are used to indicate amorphous (circle) or semi-crystalline (triangle) state of polymer

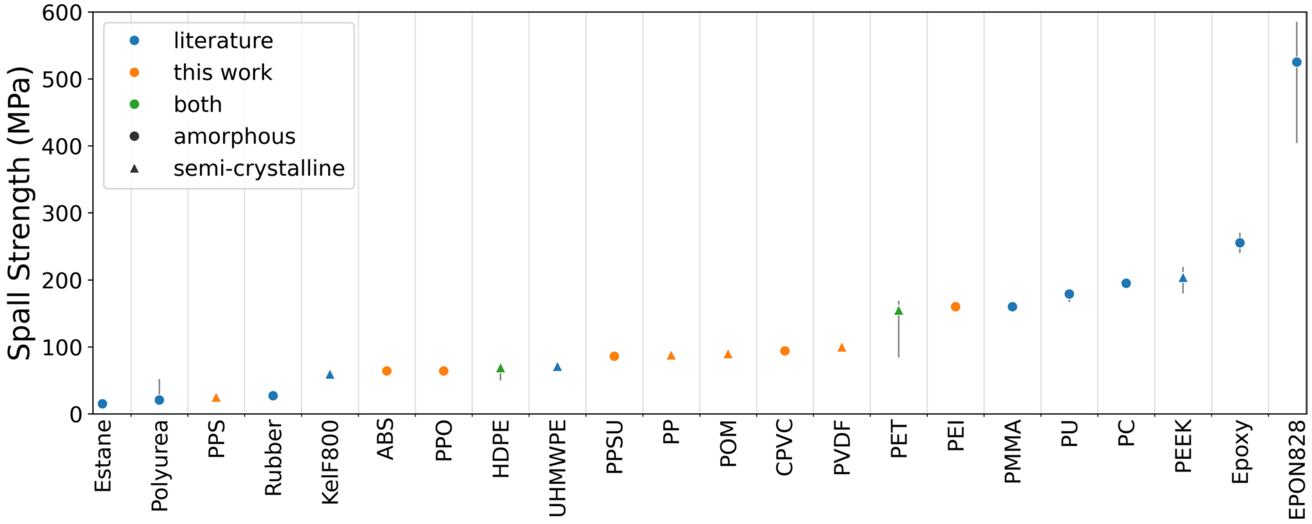

Fig. 5 Median spall strength of 23 different polymers plotted with increasing values from left to right. Different symbols are used to indicate amorphous (circle) or semi-crystalline (triangle) state of polymer. The bars indicate the range of data from varying experimental conditions, including impact velocity, and flyer or target thickness

polymers sourced from literature and the current work (plotted from lowest to highest value). It includes thermoset polymers, like epoxies, in addition to various thermoplastic polymers. Thermosetting epoxies have the highest spall strength of ~ 525 MPa (median value that varies with impact conditions), while thermoplastic Estane is on the opposite end of the spectrum, having a spall strength of only a few MPa.

We considered various physical and mechanical (elastic/plastic) property attributes to determine if the spall strength of polymers correlates with any singular material property, beyond the bulk modulus and quasi-static yield strength, which are the two properties considered in Grady's model for calculation of the theoretical spall strength. Figure 6 plots the spall strengths correlated with various quasi-static strength properties (ultimate, tensile yield, and compressive yield strength), elastic properties (bulk, shear, and Young's modulus), Izod impact energy for fracture, and physical properties (melt and glass transition temperatures). The data, including the spall strength values of over 20 polymers, are compiled in Table 3 in the Appendix. In general, increasing quasi-static strengths, shear and Young's moduli, glass transition temperature, melting temperature, and fracture energy result in higher values of the spall strength. The Pearson correlation coefficient ($\boldsymbol{r}$) confirms this with positive coefficients, although the values tend to be low ($r = 0.2$–0.4). The highest Pearson correlation coefficient is 0.787 for the Izod impact energy.

It is also seen that the spall strength of polymers is typically higher than the corresponding values of the quasi-static tensile and compressive yield strengths and the ultimate tensile strength. Exceptions include polymers such as Estane, polyurea, PPS, and rubber, which have very low values of spall strength. Values of the spall strength also appear to be about 30–50% of the bulk modulus and the Young's modulus, with the exception of two-part epoxies such as those created by polymerizing the EPON 828 resin, whose spall strength is about 90% of the bulk modulus and only slightly higher than the value of the Young's modulus. Estane and polyurea are other exceptions, having spall strengths that are a small fraction of the bulk and Young's moduli.

In order to map the response of the various semi-crystalline and amorphous thermoplastic and thermosetting polymers to their dynamic tensile failure response, we correlated the normalized spall strength (with respect to the ideal spall strength) as a function of the decompression (tensile) strain rate, which represents the rate of material expansion during unloading. Values of the ideal strength were calculated based on the equation defined by Kanel et al. [29] given by Eq. (5), where $\boldsymbol{\rho}_0$ is density, and $\boldsymbol{C}_0$ and $\boldsymbol{b}$ are coefficients (obtained from literature) of the linear equation of state of the form: $\boldsymbol{U_s} = \boldsymbol{C}_0 + \boldsymbol{b}\boldsymbol{u_p}$ [16], where $\boldsymbol{U_s}$ and $\boldsymbol{u_p}$ are respectively the shock and particle velocities.

$$\sigma_{id} = \frac{\rho_0 C_0^2}{4b} \tag{5}$$

Figure 7 shows the normalized values of the spall strength ($\boldsymbol{\sigma_{sp}/\sigma_{id}}$) for various polymers plotted as a function of the decompression strain rate. Common metals, including FCC Al and Cu, as well as BCC Fe and Mo, are also included (for comparison purposes), showing increasing spall strength with increasing decompression strain rate. For most polymers, the spall strength is shown for singular values of the decompression strain rate. Epoxy (XB3485 resin and 3486 hardener) and PMMA are two polymers for which the spall strength data are available for several decompression strain rates, showing the normalized spall strength increasing with increasing decompression strain rate. It can be seen that, in general, polymers exhibit spall strengths that are up to about 20% of their ideal strength. This is similar to that of the metals (at similar decompression strain rates) included in the comparison. Two-part epoxies using EPON 828 as the resin exhibit spall strength almost 60% of the ideal strength under dynamic tensile loading. There is no obvious trend illustrating differences in the spall failure response for semi-crystalline versus amorphous polymers.

The mapping of the normalized spall strengths (obtained from measurements of free surface velocity profiles) with respect to the idealized strength of polymers as a function of the decompression (tensile) strain rate shows a wide range of tensile failure responses. It does not, however, provide direct correlation of failure processes associated with different polymer systems. In order to develop the necessary correlations among different polymeric systems, time-resolved diagnostics of structural changes leading to void/crack initiation prior to spall failure are necessary. In-depth MD simulations of amorphous and semi-crystalline polymers may also aid the understanding of spall failure initiation and the correlation of spall strength with increasing impact stress and tensile strain rate.

Conclusions

The dynamic tensile spall failure strength of several commercially available polymers is experimentally determined, adding to those for which their values are available in the literature. Plate-on-plate impact experiments using multi-sample target configurations with a single-stage gas gun are used to determine the spall strengths from sample back free surface velocity profiles captured using PDV interferometry. The measured velocity profiles generally reveal similar signatures of the high-pressure state, unloading, and velocity pullback associated with spall failure, indicating no obvious effects of process-related anisotropy or impact stress. Values of the spall strengths calculated from the velocity profiles

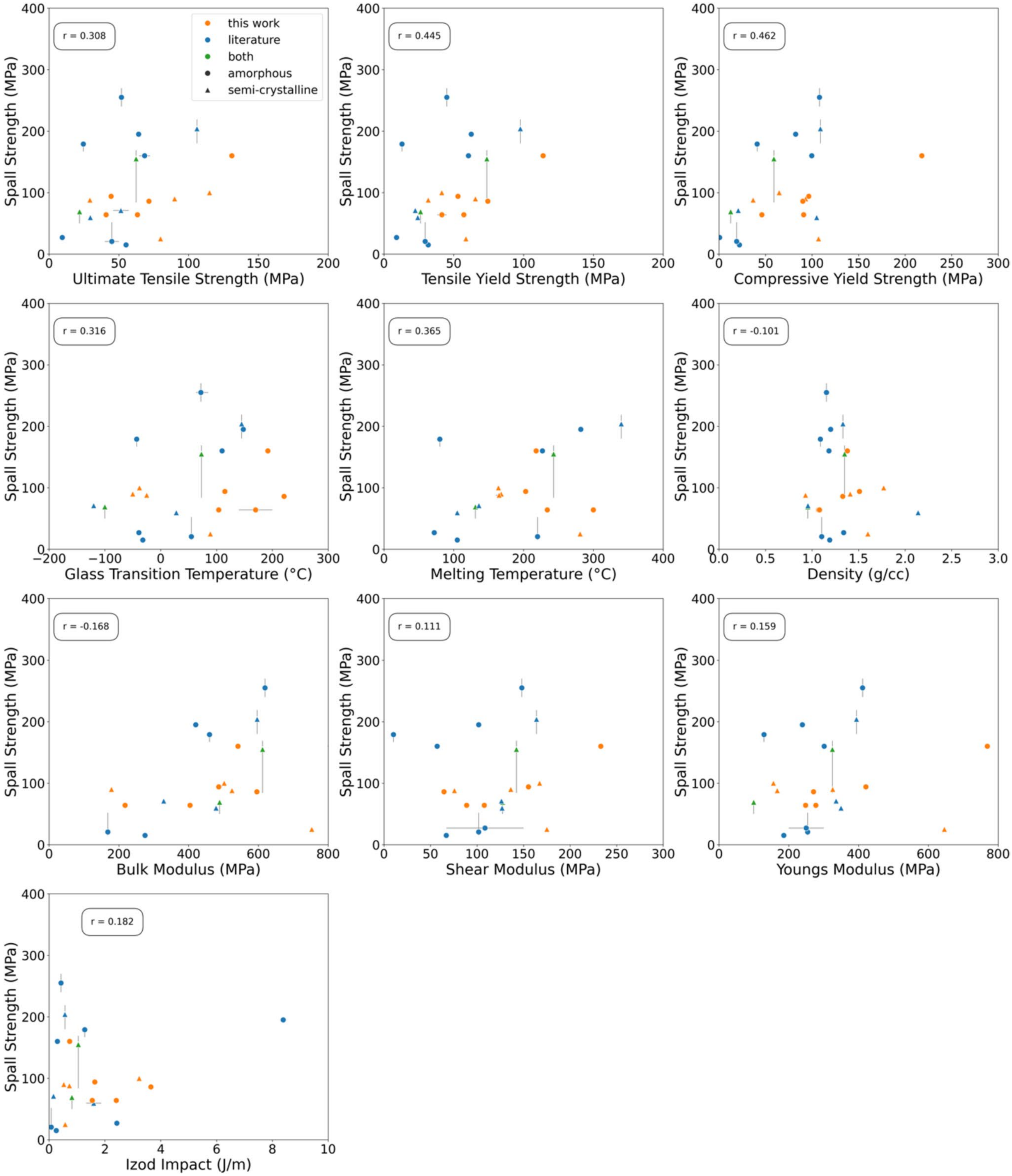

Fig. 6 Spall strength plotted against various strength, fracture, elastic, and physical properties. Different symbols are used to indicate amorphous (circle) or semi-crystalline (triangle) state of polymer. The Pearson correlation coefficient (*r*) is annotated in each plot. For the most part, spall strength values scale with the other properties. Two-part epoxies such as those created by polymerizing the EPON 828 resin fall outside many of the ranges due to its high spall strength value, so it has not been included

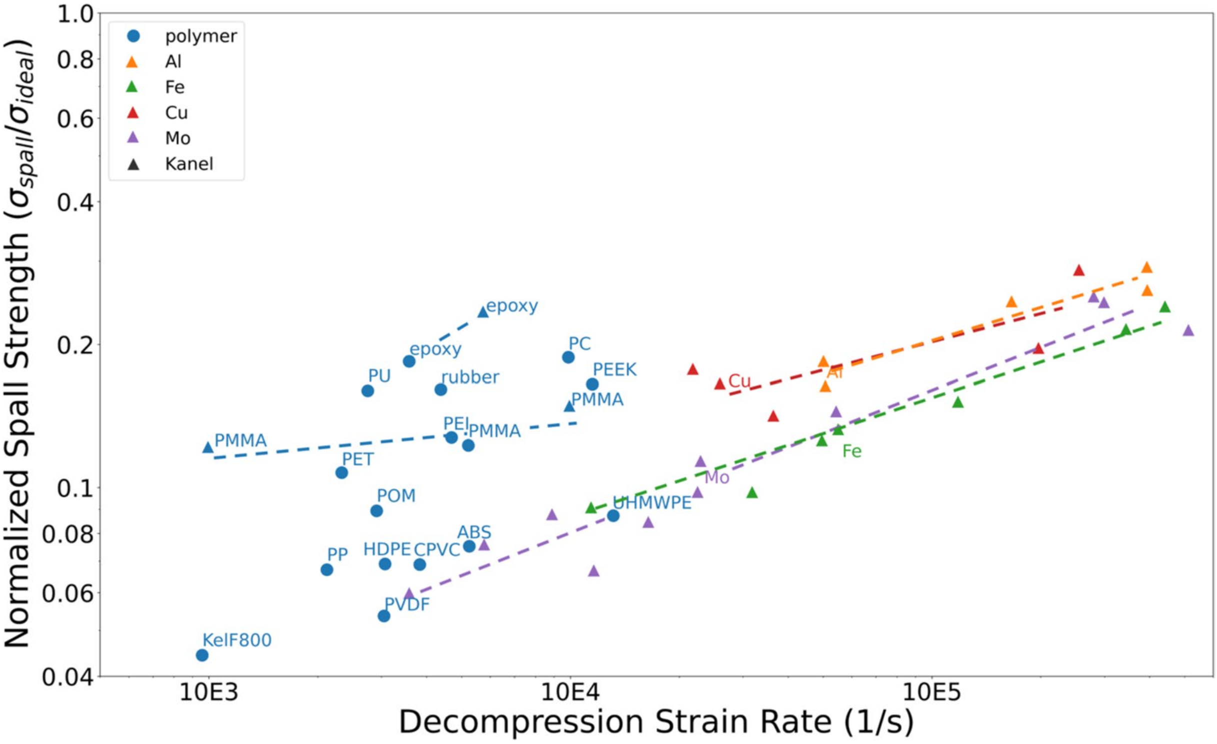

Fig. 7 Spall strength/ideal strength versus strain rate for various polymers and metals. Polymers are shown in blue, Al is orange, Fe is green, Cu is red, and Mo is purple. Data indicated by triangles come from Kanel [16]. Guidelines have been drawn to show the trends of those materials with multiple data points (Color figure online)

measured for the various polymers range between 25 and 160 MPa, with no direct correlation to inherent characteristics, including amorphous/semi-crystalline structure. The calculated spall strengths, correlated with a model for theoretically predicted spall strength values, provides the void volume fraction at spall being in the range of 0.01 to 0.35, unlike the constant value of 0.15 common for ductile metals and alloys. The database of the spall strengths of 23 unique polymers (experimentally determined in this work combined with those available in the literature) along with readily available mechanical and physical properties shows no direct correlation with specific physical and mechanical properties, although the spall strength of most polymers is typically higher than the corresponding quasi-static compressive and tensile strength values and about 30–50% of the bulk and elastic moduli, with some exceptions. Spall strengths of the various polymers normalized with respect to their calculated idealized strength and correlated with the decompression (tensile) strain rate reveal consistent trends to those for metals and alloys (with normalized spall strengths nominally 20% of idealized strength), although no obvious distinction between the dynamic tensile spall failure response of the various polymer types, including thermoplastic amorphous and semi-crystalline polymers, is observed.

Appendix: Database of Median Spall Strength and Mechanical and Physical Properties of Polymers

See Table 3.

Table 3 Database of median spall strength and mechanical and physical properties of polymers

Material	σ_{sp} (MPa)	σ_{UTS} (MPa)	$\sigma_{y,tens}$ (MPa)	$\sigma_{y,comp}$ (MPa)	T_g $(°C)$	T_m $(°C)$	ρ (g/cm^3)	$Izod$ (J/m)	K (GPa)	G (GPa)	E (GPa)
ABS	64	41	42	46	104	234	1.07	2.41	404	89	248
CPVC	94	45	53	97	115	203	1.51	1.64	486	155	421
EPON 828-A[a]	525	65	69	76	175	N/A	1.19	22.43	102	102	265
EPON 828-B[b]	365	59	69	76	175	N/A	1.19	22.43	207	110	285
Epoxy[c]	255	52	45	108	72	N/A	1.19	0.43	619	148	412
Estane	15	55	32	22	− 32	105	1.19	0.26	275	67	186
HDPE	69	22	26	13	− 100	131	0.95	0.82	489	127	100
Kel F 800	60	30	24	105	28	105	2.14	1.60	479	127	350
PC	195	64	63	82	148	282	1.20	8.39	421	102	239
PEEK	204	106	98	109	145	340	1.34	0.57	596	164	394
PEI	160	131	114	218	192	218	1.38	0.74	542	233	769
PET	155	62	74	59	73	243	1.36	1.05	612	142	325
Polyurea	21	45	30	19	55	220	1.10	0.08	169	102	254
PMMA	160	69	61	100	110	227	1.19	0.30	806	57	302
POM	90	90	66	93	− 50	168	1.41	0.53	179	136	326
PP	88	29	32	37	− 25	165	0.93	0.73	524	76	167
PPO	64	63	57	91	170	300	1.08	1.55	218	108	278
PPS	25	80	59	107	89	281	1.60	0.58	753	175	646
PPSU	86	72	74	90	221	N/A	1.33	3.65	596	65	271
PU	179	25	13	41	− 43	80	1.09	1.28	460	10	129
PVDF	100	115	41	65	− 38	164	1.77	3.23	502	167	156
Rubber	27	9	9	1	− 39	72	1.34	2.43	4167	109	250
UHMWPE	71	52	22	21	− 120	136	0.96	0.16	329	126	336

[a] EPON 828 resin and EPIKURE 3223 hardener

[b] EPON 828 resin and EPIKURE 3233 hardener

[c] XB3485 resin and 3486 hardener

Acknowledgements This work was supported in part by the Defense Threat Reduction Agency (DTRA) Project No. HDTRA1-18-1-0004). KGF acknowledges the fellowship provided by the National Defense Science & Engineering Graduate (NDSEG) Program.

Data availability All data will be available upon request.

Declarations

Conflict of interest On behalf of all authors, the corresponding author states that there is no conflict of interest.

Open Access This article is licensed under a Creative Commons Attribution 4.0 International License, which permits use, sharing, adaptation, distribution and reproduction in any medium or format, as long as you give appropriate credit to the original author(s) and the source, provide a link to the Creative Commons licence, and indicate if changes were made. The images or other third party material in this article are included in the article's Creative Commons licence, unless indicated otherwise in a credit line to the material. If material is not included in the article's Creative Commons licence and your intended use is not permitted by statutory regulation or exceeds the permitted use, you will need to obtain permission directly from the copyright holder. To view a copy of this licence, visit http://creativecommons.org/licenses/by/4.0/.

References

1. Grady DE (1988) The spall strength of condensed matter. J Mech Phys Solids 36(3):353–384. https://doi.org/10.1016/0022-5096(88)90015-4
2. Hazell PJ, Appleby-Thomas GJ, Wielewski E, Escobedo JP (2014) The shock and spall response of three industrially important hexagonal close-packed metals: magnesium, titanium and zirconium. Phil Trans R Soc A 372:20130204. https://doi.org/10.1098/rsta.2013.0204
3. Meyers MA, Aimone CT (1983) Dynamic fracture (spalling) of metals. Prog Mater Sci 28(1):1–96. https://doi.org/10.1016/0079-6425(83)90003-8
4. Antoun T (2003) Spall fracture. Springer-Verlag
5. Meyers MA (1994) Dynamic behavior of materials. Wiley Online Books
6. Davison L, Grady DE, Shahinpoor M (2012) High-pressure shock compression of solids II: dynamic fracture and fragmentation. Springer
7. Jones DR, Fensin SJ, Dippo O, Beal RA, Livescu V, Martinez DT, Trujillo CP, Florando JN, Kumar M, Gray GT III (2016) Spall fracture in additive manufactured Ti–6Al–4V. J Appl Phys 120(13):135902. https://doi.org/10.1063/1.4963279
8. Bragov AM, Balandin VV, Ayu K, Lomunov AK, Vorobtsov IV, Kuznetsov AV, Savenkoy GG (2017) High-rate deformation and spall fracture of some metals. Procedia Eng 197:260–269. https://doi.org/10.1016/j.proeng.2017.08.103

9. Fensin SJ, Valone SM, Cerreta EK, Escobedo-Diaz JP, Gray GT III, Kang K, Wang J (2013) Effect of grain boundary structure on plastic deformation during shock compression using molecular dynamics. Model Simul Mater Sci Eng 21:015011. https://doi.org/10.1088/0965-0393/21/1/015011
10. Lorenzana HE, Belak JF, Bradley KS, Bringa EM, Budil KS, Cazamias JU, El-Dasher B, Hawreliak JA, Hessler J, KadauK KDH, McNaney JM, Milathianaki D, Rosolankova K, Swift DF, Taravillo M, Van Buuren TW, Wark JS, de la Rubia TD (2008) Shocked materials at the intersection of experiment and simulation. Sci Model Simul SMNS 15(1):159–186. https://doi.org/10.1007/s10820-008-9107-z
11. Golubev VK, Novikov SA, Sobolev YS (1982) Spalling failure of Plexiglas, Teflon, and polyethylene at normal and elevated temperatures. Strength Mater 14(2):234–237. https://doi.org/10.1007/BF00769063
12. Golubev VK, Novikov SA, Sobolev YS (1982) Effect of temperature on spall of polymeric materials. J Appl Mech Tech Phys 23(1):134–141. https://doi.org/10.1007/BF00911992
13. Bie BX, Pan RC, Xu J, Chai HW, Chen S, Du GH, Bian YL, Cai Y, Luo SN (2023) Dynamic compression and fracture of poly(ether-ether-ketone) under plate impact. Int J Mech Sci 246:108138. https://doi.org/10.1016/j.ijmecsci.2023.108138
14. Geras'kin AA, Khishchenko KV, Krasyuk IK, Pashinin PP, Semenov AY, Vovchenko VI (2009) Specific features of spallation processes in polymethyl methacrylate under high strain rate. Contrib Plasma Phys 49:451–454. https://doi.org/10.1002/ctpp.200910044
15. Bourne NK (2016) On the shock response of polymers to extreme loading. J Dyn Behav Mater 2(1):33–42. https://doi.org/10.1007/s40870-016-0055-5
16. Kanel GI (2010) Spall fracture: methodological aspects, mechanisms and governing factors. Int J Fract 163(1–2):173–191. https://doi.org/10.1007/s10704-009-9438-0
17. Bourne NK, Gray GT (2005) Dynamic response of binders; teflon, estane™ and Kel-F-800™. J Appl Phys 98(12):123503. https://doi.org/10.1063/1.2143118
18. Pepper JE, Huneault J, Rahmat M, Ashrafi B, Petel OE (2018) The effect of curing agent on the dynamic tensile failure of an epoxy subjected to plate impact. Int J Impact Eng 113:203–211. https://doi.org/10.1016/j.ijimpeng.2017.11.009
19. Jordan JL, Dattelbaum DM, Schilling BF, Welch CF, Stull JA (2018) Low pressure shock response and dynamic failure of high density polyethylene (HDPE). AIP Conf Proc. https://doi.org/10.1063/1.5044863
20. Dattelbaum DM, Schilling BF, Clements BE, Jordan JL, Welch CF, Stull JA (2024) Shock response and dynamic failure of high density-(HDPE) and ultra-high molecular weight polyethylene (UHMWPE). J Dyn Behav Mater. https://doi.org/10.1007/s40870-024-00411-3
21. Han PF, Fan D, Cai Y et al (2024) Shock and spallation behavior of ultrahigh molecular weight polyethylene. Int J Mech Sci 267:108984. https://doi.org/10.1016/j.ijmecsci.2024.108984
22. Dewapriya MAN, Miller RE (2021) Molecular-level investigation on the spallation of polyurea. MRS Commun 11(4):532–538. https://doi.org/10.1557/s43579-021-00073-5
23. Dewapriya MAN, Miller RE (2021) Molecular dynamics simulations of shock propagation and spallation in amorphous polymers. J Appl Mech. https://doi.org/10.1115/1.4051238
24. Dewapriya MAN, Miller RE (2022) Molecular dynamics study on the shock induced spallation of polyethylene. J Appl Phys 131(2):025102. https://doi.org/10.1063/5.0072249
25. Bian YL, Chai HW, Ye SJ, Xie HL, Yao XH, Cai Y (2021) Compression and spallation properties of polyethylene terephthalate under plate impact loading. Int J Mech Sci 211:106736. https://doi.org/10.1016/j.ijmecsci.2021.106736
26. Zeng F, Sun Y, Zhou Y, Li Q (2011) A molecular dynamics simulation study to investigate the elastic properties of PVDF and POSS nanocomposites. Model Simul Mater Sci Eng 19(2):025005. https://doi.org/10.1088/0965-0393/19/2/025005
27. Voorhees TJ. High-precision measurements and modeling of how brittle granular materials behave under shock compression. PhD thesis. Published online November 23, 2020. http://hdl.handle.net/1853/64148
28. Turley WD, Fensin SJ, Hixson RS et al (2018) Spall response of single-crystal copper. J Appl Phys 123(5):055102. https://doi.org/10.1063/1.5012267
29. McQueen RG, Marsh SP (1962) Ultimate yield strength of copper. J Appl Phys 33(2):654–665. https://doi.org/10.1063/1.1702483

Publisher's Note Springer Nature remains neutral with regard to jurisdictional claims in published maps and institutional affiliations.